Valence-subband structures of GaAs/$Al_xGa_{1-x}As$ quantum wires: The effect of split-off bands

D. S. Citrin and Yia-Chung Chang
Department of Physics and Materials Research Laboratory, University of Illinois at Urbana-Champaign, Urbana, Illinois 61801
(Received 5 April 1989)

The valence-subband dispersion for GaAs quantum wires in $Al_xGa_{1-x}As$ host material is calculated in a coupled-band effective-mass model in which the split-off bands are included. We derive the symmetry-adapted basis functions valid at all **k** for quantum wires of square and rectangular cross sections. Coupling to the split-off bands is seen to leave the uppermost valence subband largely unaffected near the zone center while the other subbands are more markedly affected. This is in contrast to the case of quantum wells where only the light-hole subbands are coupled to the split-off subbands at the zone center.

INTRODUCTION

In the recent past improved techniques in microfabrication have led to the development of several new ultrasmall semiconducting structures.[1-6] In turn, predictions of high carrier mobilities in quasi-one-dimensional structures, or quantum wires (QWR's), have provided an impetus for further developments in fabrication. Several such calculations[7-13] predict enhanced carrier mobilities for certain QWR designs thus opening possibilities of new applications in devices.

Recently papers have appeared in the literature dealing with the conduction-subband dispersion in GaAs/$Al_xGa_{1-x}As$ QWR's. Using a pseudopotential scheme it was found[14,15] that for thick QWR's ($>100\times100$ Å^2) the infinite-well model is valid for the lowest energy level. In this model, the x and y dependence of the wave function are independent. For thinner wires, all levels are affected by coupling between the two directions perpendicular to the QWR. The valence-subband dispersion has also been calculated, focusing on its dependence on QWR cross-sectional size,[16] in the infinite-depth potential-well limit,[17] and as a function of crossed electric and magnetic fields perpendicular to the QWR axis.[18] Excitonic properties associated with the lowest conduction and the uppermost valence subbands have also been calculated.[19] All of these calculations begin with the Luttinger-Kohn Hamiltonian[20] neglecting the split-off bands and using a spherical approximation[21] in which γ_2 and γ_3 are set equal to an average value. Recently though, optical transitions involving the split-off bands in GaAs/$Al_xGa_{1-x}As$ superlattices have been observed in photoluminescence-excitation spectroscopy[22] and in electroreflectance experiments.[23] Thus it is of interest to investigate how the split-off subbands affect the upper valence subbands for the QWR by coupling the bulk Γ_7 split-off bands to the bulk Γ_8 bands. For the QWR the coupling at the zone center is more complicated than for the quantum well (QWL). It is shown in this paper that inclusion of the split-off bands in the calculation leads to effects in the dispersion of the valence subbands, while giving approximately the same result as the infinite spin-orbit splitting model for the uppermost subband.

In this study we calculate the valence-subband dispersion for a GaAs QWR embedded in $Al_xGa_{1-x}As$ barrier material. We employ a coupled-band effective-mass equation which, unlike published results,[16-18] includes the two bulk Γ_7 split-off bands as well as the four bulk Γ_8 bands which we solve by the Rayleigh-Ritz variational principle. Thus the treatment is additionally applicable to systems with small spin-orbit splitting. Also our treatment does not make use of the spherical or axial approximations. The material parameters of GaAs are used throughout. Since we treat only small Al concentrations, we expect this to be a good approximation. We use a phenomenological two-dimensional square-well potential to model the hole confinement.

CHOICE OF BASIS

We consider a QWR in the effective-mass approximation. The QWR we treat has a rectangular cross section with sides of length W_x and W_y and has its axis in the [001] (henceforth z) direction. The Kane Hamiltonian[24] with spin-orbit coupling is adapted to include the effects of the hole confinement,

$$H=\begin{bmatrix} H_{kp} & 0 \\ 0 & H_{kp} \end{bmatrix}+H_{so}+V(x,y)\begin{bmatrix} I & 0 \\ 0 & I \end{bmatrix}, \tag{1}$$

where

$$H_{kp}=\begin{bmatrix} Ak_x^2+B(k_y^2+k_z^2) & Ck_xk_y & Ck_xk_z \\ Ck_xk_y & Ak_y^2+B(k_x^2+k_z^2) & Ck_yk_z \\ Ck_xk_z & Ck_yk_z & Ak_z^2+B(k_x^2+k_y^2) \end{bmatrix},$$

$$k_x=-i\hbar\frac{\partial}{\partial x},\quad k_y=-i\hbar\frac{\partial}{\partial y},$$

and

$$H_{so}=-\frac{\Delta}{3}\begin{bmatrix} 0 & i & 0 & 0 & 0 & -1 \\ -i & 0 & 0 & 0 & 0 & i \\ 0 & 0 & 0 & 1 & -i & 0 \\ 0 & 0 & 1 & 0 & -i & 0 \\ 0 & 0 & i & i & 0 & 0 \\ -1 & i & 0 & 0 & 0 & 0 \end{bmatrix}.$$

I is the 3×3 unit matrix and Δ is the spin-orbit splitting parameter. A, B, and C are expressible in terms of the Luttinger parameters via the relations $A=\hbar^2/2m(4\gamma_2+\gamma_1)$, $B=\hbar^2/2m(\gamma_2-2\gamma_1)$, and $C=(\hbar^2/2m)6\gamma_3$, m being the free-electron mass. The Hamiltonian is written in the basis of p-like states $|X\rangle\uparrow$, $|Y\rangle\uparrow$, $|Z\rangle\uparrow$, $|X\rangle\downarrow$, $|Y\rangle\downarrow$, $|Z\rangle\downarrow$, where $|X\rangle$ transforms like p_x, etc. The confining potential for the holes is

$$V(x,y)=\begin{cases} 0 & \text{for } |x|<W_x/2 \text{ and } |y|<W_y/2 \\ V_0 & \text{for } |x|\geq W_x/2 \text{ or } |y|\geq W_y/2 \end{cases}, \quad (2)$$

where V_0 is the valence-band discontinuity between the QWR material and the barrier material. The barrier height as a function of Al concentration x is $V_0=Q_h\Delta E_g(x)$ (Ref. 25), where $\Delta E_g(x)=1.155x+0.37x^2$ eV (Ref. 26) is the difference in band gaps at $\mathbf{k}=\mathbf{0}$ between the GaAs and the $Al_xGa_{1-x}As$ and $Q_h=0.4$ is the fraction of the band-gap mismatch in the valence bands.

Next we discuss the basis functions for QWR's of square and of rectangular cross sections. For the QWL grown in the [001] direction, the envelope function depends only on z. In the case of the QWR, the envelope function depends on x and y. Hence, if we need to expand the QWL envelope function in a basis truncated at n terms, we expect to have to expand the QWR envelope function in n^2 terms to attain comparable accuracy. Consequently, it is necessary computationally to use the symmetry of the system in order to block diagonalize the Hamiltonian, the details of which are presented below. It is important here to point out a major difference in the utility of the group theoretical treatments of the QWL and the QWR. Only for $\mathbf{k}=\mathbf{0}$ and for $\mathbf{k}$ along certain special directions is the symmetry of the QWL high. In these directions the subbands are easily calculated. For arbitrary $\mathbf{k}$ the symmetry of the system is low and states of different symmetries along special directions are coupled by the Hamiltonian. For the QWR, we consider the system in general for arbitrary $\mathbf{k}$, since all $\mathbf{k}$ already lie on a symmetry axis of the QWR—a fourfold axis for the QWR of square cross section or a twofold axis for the QWR of rectangular cross section.

For the present let $W_x=W_y$ so that the cross section of the QWR is a square. We consider this case first because it is computationally easier than the QWR of rectangular cross section and also for the insight it provides into the more general case to be considered later. Because the confining potential for the QWR of square cross section has the symmetry of the C_{4v} point group, we expect to be able to expand the envelope function as linear combinations of functions transforming like $R(\Gamma_1)$, $S_z(\Gamma_2)$, $x^2-y^2(\Gamma_3)$, $xy(\Gamma_4)$, and $x,y(\Gamma_5)$. (See Ref. 27 for an explanation of these symbols.) Each term of the effective-mass wave function, then, can be written as a product of a spatial factor having Γ_1, Γ_2, Γ_3, Γ_4, or Γ_5 symmetry, one of the p-like $|X\rangle$, $|Y\rangle$, or $|Z\rangle$ orbitals, and a spin-$\frac{1}{2}$ spinor. This gives $6\times3\times2=36$ types of terms. By utilizing the theory of point groups, the Hamiltonian can be block diagonalized into two pairs of 9×9 blocks, each pair with Γ_6 or Γ_7 symmetry being degenerate, thus reducing the size of the eigenvalue problems to be solved. In the limit of infinite spin-orbit coupling the situation is

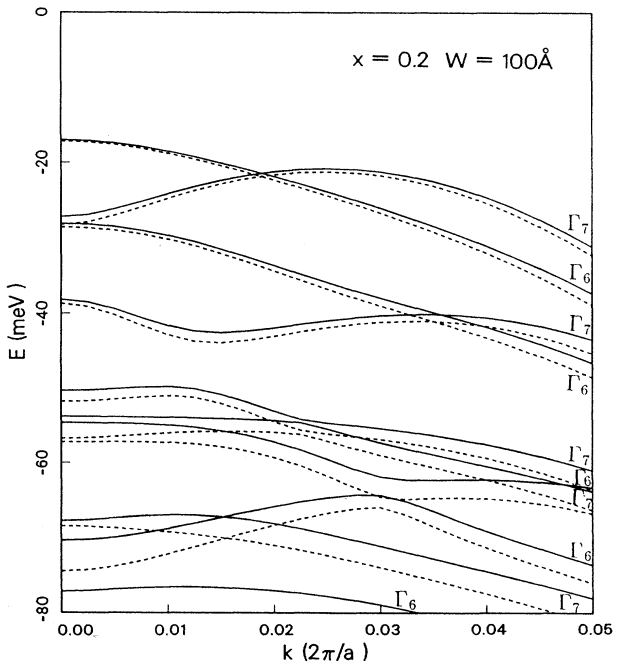

FIG. 1. Valence-subband dispersion in the [001] direction for a $GaAs/Al_{0.2}Ga_{0.8}As$ QWR of square cross section with sides of length $W=100$ Å. Solid curves are for $\Delta=340$ meV, dashed curves for $\Delta=\infty$. The symmetries of the subbands are as indicated. The zero of energy is taken at the bottom of the potential well.

further simplified in that the Hamiltonian reduces to two pairs of 6×6 blocks and two pairs of 3×3 blocks, the latter giving the split-off bands.

The product under consideration is $(\Gamma_1\oplus\Gamma_2\oplus\Gamma_3\oplus\Gamma_4\oplus\Gamma_5)\otimes(\Gamma_1\oplus\Gamma_5)\otimes\Gamma_6$, where the first factor is for the envelope functions, the second factor for the p-like orbitals, and the last factor for the spin-$\frac{1}{2}$ spinors. This product gives bases of $\Gamma_6^{1/2}$, $\Gamma_6^{-1/2}$, $\Gamma_7^{1/2}$, and $\Gamma_7^{-1/2}$ symmetries. The $\Gamma_6^{1/2}$ and $\Gamma_6^{-1/2}$ subbands are Kramers degenerate as are the $\Gamma_7^{1/2}$ and $\Gamma_7^{-1/2}$ subbands. Since the $\Gamma_7^{1/2}$ basis is easily obtained from the $\Gamma_6^{1/2}$ basis by a simple change of symbols, we shall only consider the $\Gamma_6^{1/2}$ basis. Using the notation and tables of Ref. 27, we obtain the following $\Gamma_6^{1/2}$ basis states:

$$\frac{1}{\sqrt{2}}\begin{bmatrix}y\\-x\\0\\0\\0\\0\end{bmatrix},\quad \frac{i}{\sqrt{2}}\begin{bmatrix}x\\y\\0\\0\\0\\0\end{bmatrix},\quad \frac{ix-y}{\sqrt{2}}\begin{bmatrix}0\\0\\0\\0\\0\\1\end{bmatrix},$$

$$\begin{bmatrix}0\\0\\R\\0\\0\\0\end{bmatrix},\quad \frac{iR}{\sqrt{2}}\begin{bmatrix}0\\0\\0\\i\\-1\\0\end{bmatrix},\quad \frac{ixy}{\sqrt{2}}\begin{bmatrix}0\\0\\0\\-1\\i\\0\end{bmatrix},\qquad (3)$$

$$\frac{-i}{\sqrt{2}}\begin{bmatrix}0\\0\\S_z\\0\\0\\0\end{bmatrix},\quad \frac{S_z}{2}\begin{bmatrix}0\\0\\0\\i\\-1\\0\end{bmatrix},\quad \frac{x^2-y^2}{2}\begin{bmatrix}0\\0\\0\\-1\\i\\0\end{bmatrix},$$

where the components of the six-dimensional column vectors are $|X\rangle\uparrow$, $|Y\rangle\uparrow$, $|Z\rangle\uparrow$, $|X\rangle\downarrow$, $|Y\rangle\downarrow$, $|Z\rangle\downarrow$. The $\Gamma_7^{1/2}$ basis states are obtained by interchanging $R\leftrightarrow xy$, $S_z\leftrightarrow x^2-y^2$, and $x\leftrightarrow y$.

We now consider a QWR of rectangular cross section so that we now allow for $W_x\neq W_y$. With the change in cross section from square to rectangular, the symmetry is reduced to C_{2v}. The basis states are now of $\Gamma_5^{1/2}$ symmetry. The C_{2v} basis states are the previously described C_{4v} basis states of $\Gamma_6^{1/2}$ symmetry of expression (3) together with the basis states of $\Gamma_7^{1/2}$ symmetry. The details of the numerical computations for the matrix elements of the Hamiltonian are given in the Appendix.

The previous group theoretical treatment is valid at all $\mathbf{k}$. For the QWL (Ref. 28) the point-group symmetry is severely reduced at arbitrary $\mathbf{k}$ compared with at the zone center.

COMPUTATIONS AND RESULTS

We calculate the valence-subband dispersion for QWR's of both square and rectangular cross sections. Although the square cross section QWR is a special case of the rectangular cross section and may not be realized in practice, there are two reasons for treating the QWR of square cross section. The first is that by doing so, certain features of the subband dispersion may be attributed to the reduced dimensionality of the system. The second reason is computational; the higher the symmetry of the system, the greater the degree to which the Hamiltonian block diagonalizes. We solve the eigenvalue problem for the QWR of square cross section by truncating the summations over i and j at 7 in Eqs. (A4) and (A5) of the Appendix and choosing the β_i's to maximize (in the electron picture) the uppermost hole subband energy at each $\mathbf{k}$. In the calculation for the QWR of rectangular cross section, the summations over i and j are truncated at 5. The Raleigh-Ritz variational principle gives a lower bound (again in the electron picture) for the uppermost subband. The deeper subbands are thus less accurate than the uppermost subband.

In Fig. 1 is plotted the valence-subband dispersion for a GaAs/$Al_{0.2}Ga_{0.8}As$ QWR of square cross section with sides of length $W_x=W_y=W=100$ Å using the Luttinger parameters $\gamma_1=6.85$, $\gamma_2=2.1$, and $\gamma_3=2.9$.[29] The energies are displayed in the electron picture; they are the negative of those obtained from the Hamiltonian H. The solid curves are for $\Delta=340$ meV and the dashed curves for $\Delta=\infty$. In Fig. 2 is the valence-subband dispersion of a rectangular cross section QWR with $W_x=75$ Å and $W_y=100$ Å. Otherwise, the parameters are the same as

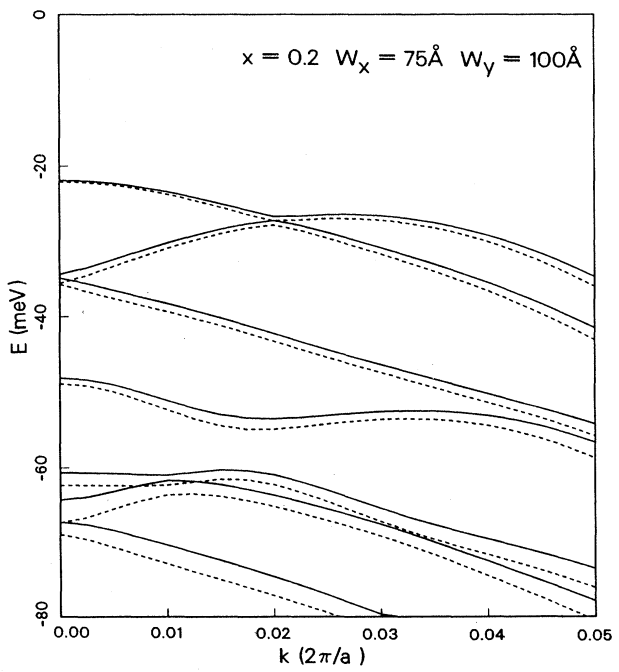

FIG. 2. Valence-subband dispersion in the [001] direction for a GaAs/$Al_{0.2}Ga_{0.8}As$ QWR of rectangular cross section with sides of lengths $W_x=75$ Å and $W_y=100$ Å. Solid curves are for $\Delta=340$ meV, dashed curves for $\Delta=\infty$. All subbands are Γ_5. The zero of energy is taken at the bottom of the potential well.

those used to obtain Fig. 1. The plots account for some of the features observed in published results of QWR valence-subband structure. The crossings between subbands of Γ_6 and Γ_7 symmetries in Fig. 1 (QWR of square cross section) are not present in Fig. 2 (QWR of rectangular cross section). The upper few subbands of Fig. 1 are qualitatively similar to those of the figures of Ref. 17 where superimposition of the plots from that reference reveals crossing subbands. The QWR treated in Ref. 17 is of circular cross section. Hence, the subbands calculated in that work can be labeled as Γ_6 and Γ_7 in the C_{4v} point group and accidental degeneracies can and in fact do occur. Figure 2 is most fruitfully compared with Fig. 2(a) of Ref. 16 in which the valence subbands for QWR's of rectangular cross section are treated. [We do not plot the valence subbands for a QWR with $W_x = 50$ Å and $W_y = 100$ Å as in Fig. 2(a) of Ref. 16 since the further the cross section deviates from square the more difficult it is to optimize the β_i's in order to assure accuracy.] The point group is now C_{2v}, all the subbands are Γ_5, and the accidental degeneracies, such as those seen in Fig. 1, are lifted. Thus, in Figs. 1 and 2 of this study and in the plots of Ref. 16, we see that the subband repulsion, for example between the upper two subbands, increases as the QWR cross section becomes more oblong. The subband dispersion progresses from pure QWR-like to QWL-like.

In order to estimate the accuracy of the results obtained by truncating the summations over i and j at 7, we calculate the zone-center hole energies truncating the summations at 11. The results for the material parameters used to obtain Fig. 1 are tabulated in Table I(a). The zone-center energies were found to be 0.4% higher for the uppermost subband ranging to 3% higher for the lowest subband shown in Fig. 1.

It is of interest to compare the effect of the inclusion of the split-off bands in QWR's and QWL's as many authors have neglected them. Nevertheless, in a paper by Eppenga, Schuurmans, and Colak,[30] the split-off subbands are included in a multiband effective-mass calculation of the subband dispersion in $GaAs/Al_xGa_{1-x}As$ QWL's. It is shown that at the zone center, heavy-hole (HH) subbands are uncoupled while light-hole (LH) subbands are coupled to the split-off subbands. This is to be expected as the 6×6 Luttinger-Kohn Hamiltonian including spin-orbit splitting[20] couples light-hole QWL subbands to the split-off subbands at the zone center whereas the heavy-hole subbands are not coupled to the split-off subbands at $\mathbf{k}=\mathbf{0}$.

In order to carry out this comparison, we calculate the valence-subband structure for a QWL for both $\Delta = 340$ meV and $\Delta = \infty$. We use the Hamiltonian of expression (1) with $k_z = -i\hbar(\partial/\partial z)$ and the basis

$$\begin{bmatrix} z \\ 0 \\ 0 \\ 0 \\ 0 \\ 0 \end{bmatrix}, \begin{bmatrix} 0 \\ z \\ 0 \\ 0 \\ 0 \\ 0 \end{bmatrix}, \begin{bmatrix} 0 \\ 0 \\ R \\ 0 \\ 0 \\ 0 \end{bmatrix}, \begin{bmatrix} 0 \\ 0 \\ 0 \\ R \\ 0 \\ 0 \end{bmatrix}, \begin{bmatrix} 0 \\ 0 \\ 0 \\ 0 \\ R \\ 0 \end{bmatrix}, \begin{bmatrix} 0 \\ 0 \\ 0 \\ 0 \\ 0 \\ z \end{bmatrix}.$$

The variational wave function is written as a sum of Gaussians,

$$\langle r|\Psi_5^{1/2}\rangle = z \sum_{n=1,2,6} w_n \sum_{i=1}^{\infty} c_n(i) e^{-\beta_i z^2} + \sum_{n=3}^{5} w_n \sum_{i=1}^{\infty} c_n(i) e^{-\beta_i z^2},$$

where w_n is a column vector with a 1 in the nth place and

TABLE I. The zone-center energies for the material parameters of Figs. 1 and 3 for $\Delta = 340$ meV and $\Delta = \infty$. Energies are in meV. Fractional energy difference in percent η is defined as $100(E_{\Delta=\infty} - E_{\Delta=340})/E_{\Delta=340}$. (a) is for a QWR with $W_x = W_y = 100$ Å. The summations over i and j are truncated at 11. (b) is for a QWL with $W = 100$ Å. The summations over i are truncated at 15.

(a)

subband	$E_{\Delta=340\text{ meV}}$	$E_{\Delta=\infty}$	η	subband	$E_{\Delta=340\text{ meV}}$	$E_{\Delta=\infty}$	η
1	−16.9	−17.1	1	6	−52.6	−55.6	6
2	−27.0	−28.1	4	7	−52.8	−55.3	5
3	−28.0	−28.5	2	8	−65.6	−66.4	1
4	−37.8	−38.4	2	9	−68.2	−72.4	6
5	−49.2	−50.8	3	10	−74.7	−80.4	8

(b)

subband	$E_{\Delta=340}$	$E_{\Delta=\infty}$	η
HH1	−6.9	−6.9	0
LH1	−19.9	−20.4	3
HH2	−27.7	−27.7	0
HH3	−59.7	−59.7	0
LH2	−70.9	−73.9	4
HH4	−96.3	−96.3	0
HH5	−98.3	−98.3	0

0's elsewhere. Truncating the summations over i at 15, we obtain the valence-subband dispersion in the [110] [Fig. 3(a)] and [100] [Fig. 3(b)] directions for a GaAs/$Al_{0.2}Ga_{0.8}As$ QWL of thickness $W=100$ Å which is comparable to the dimensions of the QWR's treated in this study. The solid curves are for $\Delta=340$ meV while the dashed ones are for $\Delta=\infty$. In Table I(b) are listed the zone-center energies for $\Delta=340$ meV and $\Delta=\infty$. Comparison of the columns labeled η, which is the fractional difference in the zone-center subband energy in percent calculated with $\Delta=340$ meV and $\Delta=\infty$, $100(E_{\Delta=340}-E_{\Delta=\infty})/E_{\Delta=340}$, for the QWR and QWL, displays the relative accuracy of the $\Delta=\infty$ approximation for the two cases. For the QWL the $\Delta=\infty$ approximation is exact at the zone center for the heavy-hole subbands; only the light-hole subbands show a sizable lowering below the value calculated for $\Delta=340$ meV.[30] On the other hand, for the QWR the inclusion of a realistic value of the spin-orbit splitting in our treatment is seen to affect all subbands at the zone center, the deep-lying subbands most strongly. The uppermost subband though is weakly affected, especially near the zone center which is the maximum in energy. Reference to the 6×6 Luttinger-Kohn Hamiltonian shows that all QWR subbands arising from the bulk Γ_7 bands are coupled to the split-off subbands at the zone center. Thus excitonic transitions involving the uppermost subbands, in which the coupling leads to a numerically small modification in the zone-center energy, are probably adequately treated using the 4×4 Luttinger-Kohn Hamiltonian. For excitonic transitions involving deeper subbands, a calculation including coupling to the split-off bands may be needed to attain high accuracy. As a consequence of coupling to the split-off subbands, structures in QWR and QWL optical spectra associated with subbands shifted ΔE by spin-orbit coupling are expected to be observed ΔE higher in energy than predicted from the infinite spin-orbit approximation.

CONCLUSION

The symmetry-adapted basis functions for QWR's of square and rectangular cross sections are derived. Unlike in the case of the QWL, where the matrix problem is reduced in size at arbitrary **k** only by exploiting Kramer's degeneracy, the QWR bases are valid at all **k**. These basis functions are used to write the Hamiltonian in the computationally convenient form H' of expression (A2) which is then used to calculate the valence subband dispersion.

As in previous studies,[16–18] strong nonparabolicities are observed in the QWR valence subbands. In contrast to the case of the QWL where at the zone center the heavy-hole and light-hole subbands are decoupled, there is strong mixing at the zone center in the case of QWR's, and so the light-hole–heavy-hole characterization is not possible, strictly speaking. It has been observed, however, that subbands may be predominantly one or the other.[17] The applicability of the light-hole–heavy-hole labels increases as W_x/W_y deviates from unity. On the other hand, in the square cross-section limit the Γ_6 and Γ_7 labels for the subbands are appropriate. As a consequence of the hybridization of heavy-hole and light-hole QWR states, the infinite spin-orbit splitting approximation is not exact at the zone center for any subband. This is in contrast to the situation for the QWL where, at the

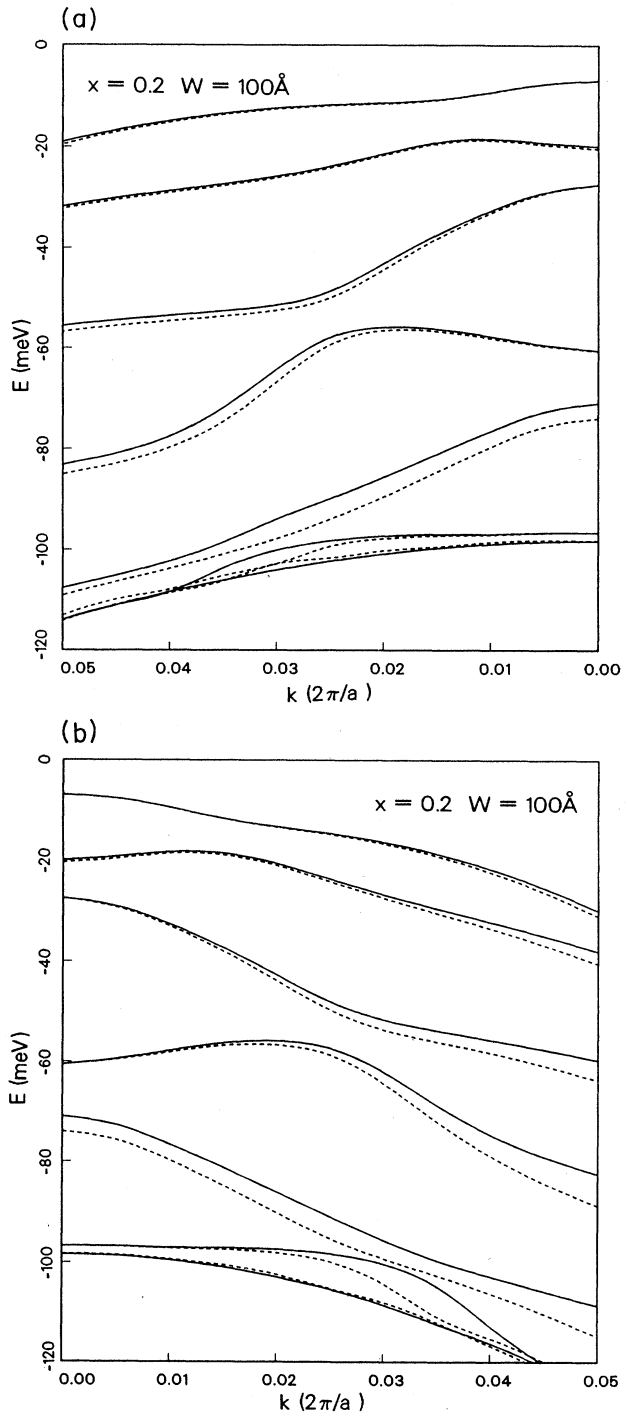

FIG. 3. Valence-subband dispersion (a) in the [110] direction and (b) in the [100] direction for a GaAs/$Al_{0.2}Ga_{0.8}As$ QWL of thickness $W=100$ Å. Solid curves are for $\Delta=340$ meV, dashed curves for $\Delta=\infty$. The zero of energy is taken at the bottom of the potential well.

zone center, the heavy-hole subbands are independent of the spin-orbit splitting. For both QWR's and QWL's, this effect is most pronounced in small structures.

A refinement of this calculation would be to account for the material parameter mismatch at the edge of the QWR potential well.[30] This would allow a careful investigation of the split-off subbands for cases where the aluminum concentration x is sufficiently large so the well depth is greater than the spin-orbit splitting. For the cases of small x treated in this study, $\Delta > V_0$ and the split-off subbands lie in the bulk Γ_8-derived continuum.

Note added in proof. The following article came to our attention after our paper was submitted: Xia Jianbai and Huang Kun, Chin. J. Semicond. **8**, 563 (1987) [Chin. Phys. **8**, 1062 (1988)]. In this work, the valence-band structures of semiconductor quantum wires were calculated in the Luttinger-Kohn effective-mass theory, excluding the split-off bands.

ACKNOWLEDGMENTS

We would like to thank G. Einevoll, A. Cancio, and H. Chu for fruitful discussions. This work was supported by the Office of Naval Research (ONR) under Contract No. N00014-89-J-1157. The use of the computing facilities of the University of Illinois Materials Research Laboratory under National Science Foundation (NSF) Grant No. NSF-DMR-86-12860 is acknowledged.

APPENDIX: CALCULATION OF MATRIX ELEMENTS

In the Appendix we give some of the details of the computation of the matrix elements. We first focus attention on the QWR of square cross section.

The envelope functions in the basis states of $\Gamma_6^{1/2}$ symmetry in expression (3) which transform like R, S_z, x^2-y^2, xy, x, and y have the following explicit forms.

For R,

$$f_+(x)g_+(y)+g_+(x)f_+(y) ,$$

for S_z,

$$f_-(x)g_-(y)-g_-(x)f_-(y), \quad f_- \neq g_-$$

for x^2-y^2,

$$f_+(x)g_+(y)-g_+(x)f_+(y), \quad f_+ \neq g_+$$

for xy,

$$f_-(x)g_-(y)+g_-(x)f_-(y) ,$$

for x,

$$f_-(x)g_+(y) ,$$

and for y,

$$f_+(x)g_-(y) ,$$

where $f_\pm$ and $g_\pm$ are functions which satisfy $f_\pm(-x)=\pm f_\pm(x)$ and $g_\pm(-x)=\pm g_\pm(x)$. The Hamiltonian matrix in the basis given in expression (3) can be written as

$$H_{nn'}=\langle \xi_n | h_{nn'} | \xi_{n'} \rangle ,$$

where the ξ_n's are envelope functions which take the following form.

For ξ_1,ξ_2,ξ_3,

$$f_+(x)g_-(y) ,$$

for ξ_4,ξ_5,

$$f_+(x)g_+(y) ,$$

for ξ_6,

$$f_-(x)g_-(y) , \tag{A1}$$

for ξ_7,ξ_8,

$$f_-(x)g_-(y), \quad f_- \neq g_-$$

and for ξ_9,

$$f_+(x)g_+(y), \quad f_+ \neq g_+ .$$

The nonvanishing entries in the upper right triangle of H contain the following operators $h_{nn'}$:

$$\begin{aligned}
h_{11} &= T_{xx} - T_{xy}\sigma + \tfrac{1}{2}(V + \sigma V \sigma) , \\
h_{12} &= -h_{13} = h_{23} = \Delta/3 , \\
h_{17} &= \eta_{xz}(1-\sigma) , \\
h_{22} &= T_{yy} + T_{xy}\sigma + \tfrac{1}{2}(V + \sigma V \sigma) , \\
h_{24} &= \eta_{yz}(1+\sigma) , \\
h_{33} &= T_{zz} + \tfrac{1}{2}(V + \sigma V \sigma) , \\
h_{35} &= -\frac{1}{\sqrt{2}}\eta_{yz}(1+\sigma) , \\
h_{36} &= -\frac{1}{\sqrt{2}}\eta_{xz}(1+\sigma) , \\
h_{38} &= \frac{1}{\sqrt{2}}\eta_{xz}(1+\sigma) , \\
h_{39} &= \frac{1}{\sqrt{2}}\eta_{yz}(1+\sigma) , \\
h_{44} &= (1+\sigma)\tfrac{1}{2}(T_{zz} + V)(1+\sigma) , \\
h_{45} &= \frac{\Delta\sqrt{2}}{3}(1+\sigma) , \\
h_{55} &= \left[\tfrac{1}{2}(T_{xx} + T_{yy}) - \frac{\Delta}{3}\right](1+\sigma) + \tfrac{1}{2}(1+\sigma)V(1+\sigma) , \\
h_{56} &= T_{xy}(1+\sigma) ,
\end{aligned} \tag{A2}$$

$$h_{59}=-h_{68}=\tfrac{1}{2}(T_{xx}-T_{yy})(1-\sigma) ,$$

$$h_{66}=\left[\tfrac{1}{2}(T_{xx}+T_{yy})+\frac{\Delta}{3}\right](1+\sigma)+\tfrac{1}{2}(1+\sigma)V(1+\sigma) ,$$

$$h_{77}=(1-\sigma)\tfrac{1}{2}(T_{zz}-V)(1-\sigma) ,$$

$$h_{78}=\frac{\Delta\sqrt{2}}{3}(1-\sigma) ,$$

$$h_{88}=\left[\tfrac{1}{2}(T_{xx}+T_{yy})-\frac{\Delta}{3}\right](1-\sigma)+\tfrac{1}{2}(1-\sigma)V(1-\sigma) ,$$

$$h_{89}=T_{xy}(1-\sigma) ,$$

$$h_{99}=\left[\tfrac{1}{2}(T_{xx}+T_{yy})+\frac{\Delta}{3}\right](1+\sigma)+\tfrac{1}{2}(1+\sigma)V(1+\sigma) ,$$

where

$$T_{\mu\mu}=Ak_\mu^2+B(k_\nu^2+k_k\lambda^2) ,$$

$$T_{\mu\nu}=Ck_\mu k_\nu \quad \text{for} \quad \mu\neq\nu ,$$

$$\eta_{\mu\nu}=-iT_{\mu\nu} ,$$

and σ is the reflection operator such that $\sigma\psi(x,y)=\psi(y,x)$.

The remainder of the entries of H are obtained from $H_{n'n}=H_{nn'}^\dagger$. Note that $\eta_{xz}^\dagger=-\eta_{xz}$ and $\eta_{yz}^\dagger=-\eta_{yz}$. The Hamiltonian H is a real symmetric matrix if $\zeta_1,\ldots,\zeta_9$ are expanded in real functions. The Hamiltonian matrix in the $\Gamma_7^{1/2}$ basis is given by

$$H'_{nn'}=\langle\xi_n|h_{nn'}|\xi_{n'}\rangle ,$$

where the envelope function ξ_n is related to ζ_n by interchanging the $+$ and $-$ subscripts of the functions $f_\pm$ and $g_\pm$ in (A1).

The basis states in expression (3) (denoted by $|i\rangle$; $i=1,\ldots,9$) form a particularly convenient representation when $\Delta=0$, for in this limit the Hamiltonian H block diagonalizes by a rearrangement of rows and columns. In the opposite limit, $\Delta\to\infty$, it is more instructive to consider a basis which diagonalizes H_{so} (where so denotes spin-orbit). This is achieved by the basis

$$\begin{aligned}&\frac{|1\rangle+|2\rangle}{\sqrt{2}},\quad |6\rangle,\quad |9\rangle,\quad \frac{\sqrt{2}|4\rangle+|5\rangle}{3} ,\\ &\frac{\sqrt{2}|7\rangle+|8\rangle}{3},\quad \frac{|2\rangle-|1\rangle+2|3\rangle}{\sqrt{6}} ,\\ &\frac{\sqrt{2}|5\rangle-|4\rangle}{3},\quad \frac{\sqrt{2}|8\rangle-|7\rangle}{3},\quad \frac{|1\rangle-|2\rangle+|3\rangle}{\sqrt{3}} .\end{aligned} \tag{A3}$$

The order of basis states in Eq. (A3) corresponds, in the notation of Ref. 20, to the $\phi_{3/2}^{(3/2)}$, $\phi_{-3/2}^{(3/2)}$, $\phi_{-3/2}^{(3/2)}$, $\phi_{1/2}^{(3/2)}$, $\phi_{1/2}^{(3/2)}$, $\phi_{-1/2}^{(3/2)}$, $\phi_{1/2}^{(1/2)}$, $\phi_{1/2}^{(1/2)}$, and $\phi_{-1/2}^{(1/2)}$ bands. The first three basis states arise from coupling to the heavy-hole bands, the next three from the light-hole bands, and the last three from the split-off bands. In the limit $\Delta\to\infty$, the latter are uncoupled from the first six states.

For the QWR of rectangular cross section, the Hamiltonian can be written in the following block form:

$$H''=\begin{bmatrix}H & \Lambda\\ \Lambda^\dagger & H'\end{bmatrix} ,$$

where H, Λ, and H' are 9×9 matrices. H and H' have identical forms as the Hamiltonian matrices for the QWR of square cross section with Γ_6 and Γ_7 symmetries, respectively. The matrix elements of Λ can be written as

$$\Lambda_{nn'}=\langle\zeta_n|\lambda_{nn'}|\xi_{n'}\rangle ,$$

where the operators $\lambda_{nn'}$ in the nonvanishing entries of Λ are given by

$$\lambda_{12}=\lambda_{21}=-\lambda_{33}=\tfrac{1}{2}(\sigma V-V\sigma) ,$$

$$\lambda_{47}=\lambda_{58}=\lambda_{69}=-\lambda_{74}^\dagger=-\lambda_{85}^\dagger=-\lambda_{96}^\dagger=\tfrac{1}{2}(1+\sigma)V(1-\sigma)$$

and the other symbols have their previously defined meanings. The upper left 9×9 block reduces to the $\Gamma_6^{1/2}$ problem for the case $W_x=W_y$ while the lower right 9×9 block reduces to the $\Gamma_7^{1/2}$ problem. The nonzero entries in the blocks Λ and $\Lambda^\dagger$ vanish for this case and the C_{4v} symmetry is restored.

Transformations analogous to those made to obtain (A3) diagonalize the spin-orbit interaction. The Hamiltonian in such a basis is rather complicated though straightforward to write down. We find that the basis change is more easily effected after solving the problem numerically.

In our calculations for QWR's of both cross sections, we work with the Hamiltonians H, H', and H'' and the envelope functions ζ_n and ξ_n. Explicitly, we expand the envelope functions entering into the $\Gamma_6^{1/2}$ wave function as

$$\begin{aligned}\zeta_n&=y\sum_{i,j=1}^{\infty}c_n(i,j)e^{-\beta_i x^2-\beta_j y^2},\quad n=1,2,3\\ \zeta_n&=\sum_{i\le j=1}^{\infty}c_n(i,j)e^{-\beta_i x^2-\beta_j y^2},\quad n=4,5\\ \zeta_6&=xy\sum_{i\le j=1}^{\infty}c_6(i,j)e^{-\beta_i x^2-\beta_j y^2} ,\\ \zeta_n&=xy\sum_{i<j=1}^{\infty}c_n(i,j)e^{-\beta_i x^2-\beta_j y^2},\quad n=7,8\\ \zeta_9&=\sum_{i<j=1}^{\infty}c_9(i,j)e^{-\beta_i x^2-\beta_j y^2} .\end{aligned} \tag{A4}$$

The envelope functions relevant to $\Gamma_7^{1/2}$ symmetry are expanded as

$$\begin{aligned}\xi_n&=x\sum_{i,j=1}^{\infty}d_n(i,j)e^{-\beta_i x^2-\beta_j y^2},\quad n=1,2,3\\ \xi_n&=xy\sum_{i\le j=1}^{\infty}d_n(i,j)e^{-\beta_i x^2-\beta_j y^2},\quad n=4,5\\ \xi_6&=\sum_{i\le j=1}^{\infty}d_6(i,j)e^{-\beta_i x^2-\beta_j y^2} ,\\ \xi_n&=\sum_{i<j=1}^{\infty}d_n(i,j)e^{-\beta_i x^2-\beta_j y^2},\quad n=7,8\\ \xi_9&=xy\sum_{i<j=1}^{\infty}d_9(i,j)e^{-\beta_i x^2-\beta_j y^2} .\end{aligned} \tag{A5}$$

Both the expansions for ζ_n and ξ_n are used for the QWR of rectangular cross section.

[1]K. Kash, A. Scherer, J. M. Worlock, H. G. Craighead, and M. C. Tamargo, Appl. Phys. Lett. **49**, 1043 (1986).
[2]H. Temkin, G. J. Dolan, M. B. Panish, and S. N. G. Chu, Appl. Phys. Lett. **50**, 413 (1987).
[3]M. A. Reed, R. T. Bate, K. Bradshaw, W. M. Duncan, W. R. Frensley, J. W. Lee, and H. D. Shih, J. Vac. Sci. Technol. B **4**, 358 (1986).
[4]P. M. Petroff, A. C. Gossard, R. A. Logan, and W. Wiegmann, Appl. Phys. Lett. **41**, 635 (1982).
[5]J. Cibert, P. M. Petroff, G. J. Dolan, D. J. Werder, S. J. Pearton, A. C. Gossard, and J. H. English, Superlatt. Microstruct. **3**, 35 (1987).
[6]M. Tsuchiya, J. M. Gaines, R. H. Yan, R. J. Simes, P. O. Holtz, L. A. Coldren, and P. M. Petroff, Phys. Rev. Lett. **52**, 466 (1989).
[7]H. Sakaki, Jpn. J. Appl. Phys. **16L**, 735 (1980).
[8]H. Sakaki, J. Vac. Sci. Technol. **19**, 148 (1981).
[9]J. Lee and H. N. Spector, J. Appl. Phys. **54**, 3921 (1983).
[10]G. Fishman, Phys. Rev. B **34**, 2394 (1986).
[11]V. K. Arora, Phys. Rev. B **23**, 5611 (1981).
[12]V. K. Arora, Phys. Status Solidi B **105**, 707 (1981).
[13]S. Briggs and J. P. Leburton, Phys. Rev. B **38**, 8163 (1988).
[14]K. B. Wong, M. Jaros, and J. P. Hagon, J. Vac. Sci. Technol. B **5**, 1198 (1987).
[15]K. B. Wong, M. Jaros, and J. P. Hagon, Phys. Rev. B **35**, 2463 (1987).
[16]J. A. Brum, G. Bastard, L. L. Chang, and L. Esaki, Superlatt. Microstruct. **3**, 47 (1987).
[17]M. Sweeny, J. Xu, and M. Shur, Superlatt. Microstruct. **4**, 623 (1988).
[18]J. A. Brum and G. Bastard, Superlatt. Microstruct. **4**, 443 (1988).
[19]I. Suemune, L. A. Coldren, and S. W. Corzine, Superlatt. Microstruct. **4**, 19 (1988).
[20]J. M. Luttinger and W. Kohn, Phys. Rev. **97**, 869 (1955).
[21]M. Alterelli, U. Ekenberg, and A. Fasolino, Phys. Rev. B **32**, 5138 (1985).
[22]J. J. Song, Y. S. Yoon, A. Fedotowsky, Y. B. Kim, J. N. Shulman, C. W. Tu, D. Huang, and H. Morkoc, Phys. Rev. B **34**, 8958 (1986).
[23]E. E. Mendez, L. L. Chang, G. Landgren, R. Ludeke, and L. Esakai, Phys. Rev. Lett. **46**, 1230 (1981).
[24]E. O. Kane, J. Phys. Chem. Solids **1**, 82 (1956).
[25]R. C. Miller, A. C. Gossard, D. A. Kleinman, and O. Munteanu, Phys. Rev. B **29**, 3740 (1984); R. C. Miller, D. A. Kleinman, and A. C. Gossard, *ibid.* **29**, 7085 (1984).
[26]H. J. Lee, L. Y Juravel, J. C. Wooley, and A. J. SpringThorpe, Phys. Rev. B **21**, 659 (1980).
[27]G. F. Koster, J. O. Dimmock, R. G. Wheeler, and H. Slatz, *Properties of the Thirty-Two Point Groups* (MIT Press, Cambridge, Mass., 1966).
[28]W. T. Masselink, Y.-C. Chang, and H. Morkoç, Phys. Rev. B **32**, 5190 (1985).
[29]K. Hess, D. Bimberg, N. O. Lipari, J. U. Fischbach, and M. Altarelli, in *Proceedings of the XIII International Conference on the Physics of Semiconductors, Rome, 1976,* edited by F. G. Fumi (North-Holland, Amsterdam, 1976), p. 142.
[30]R. Eppenga, M. F. H. Schuurmans, and S. Colak, Phys. Rev. B **36**, 1554 (1987).